



# Novel TEMPO-oxidized cellulose nanofiber/polyvinyl alcohol/polyethyleneimine nanoparticles for Cu<sup>2+</sup> removal in water

Rongrong Si · Chaojun Wu · Dongmei Yu · Qijun Ding · Ronggang Li

Received: 9 June 2021 / Accepted: 25 September 2021 / Published online: 6 October 2021  
© The Author(s), under exclusive licence to Springer Nature B.V. 2021

**Abstract** In this study, environmentally friendly TEMPO-oxidized cellulose nanofiber (TO-CNF)/polyvinyl alcohol (PVA)/polyethyleneimine (PEI) nanoparticles were obtained by assembling PEI into TO-CNF/PVA aerogel, which was prepared by freeze-drying method with the help of glutaraldehyde. FTIR results showed that PEI likely assembled into the TO-CNF/PVA aerogel due to appearances of bending vibration of the TO-CNF/PVA/PEI nanoparticles at 1615 cm<sup>-1</sup>. BET results further demonstrated that PEI have successfully assembled into the aerogel since the specific surface area (22.93 m<sup>2</sup>/g) of TO-CNF/PVA / PEI nanoparticles was lower than that (56.37 m<sup>2</sup>/g) of TO-CNF/PVA aerogel. SEM results also showed that

PEI could obviously regulate the morphology of TO-CNF/PVA aerogel. TGA indicated that TO-CNF/PVA/PEI nanoparticles were structurally stable at 216.4 °C. The adsorption kinetics of the TO-CNF/PVA/PEI nanoparticles for copper ion (Cu<sup>2+</sup>) removal presented good correlations with the Pseudo-second-order kinetic and Langmuir model ( $R^2 > 0.99$ ). Its maximum adsorption capacity for Cu<sup>2+</sup> according to Langmuir model was 156.8 mg/g. The adsorption equilibrium could reach in near one hour, and the adsorption efficiency could still maintain more than 80% after 3 cycles.

---

R. Si · C. Wu (✉) · D. Yu (✉) · Q. Ding · R. Li  
State Key Laboratory of Biobased Material and Green  
Papermaking, Qilu University of Technology (Shandong  
Academy of Sciences), Jinan 250353,  
Shandong, China  
e-mail: Chaojunwu2007@163.com

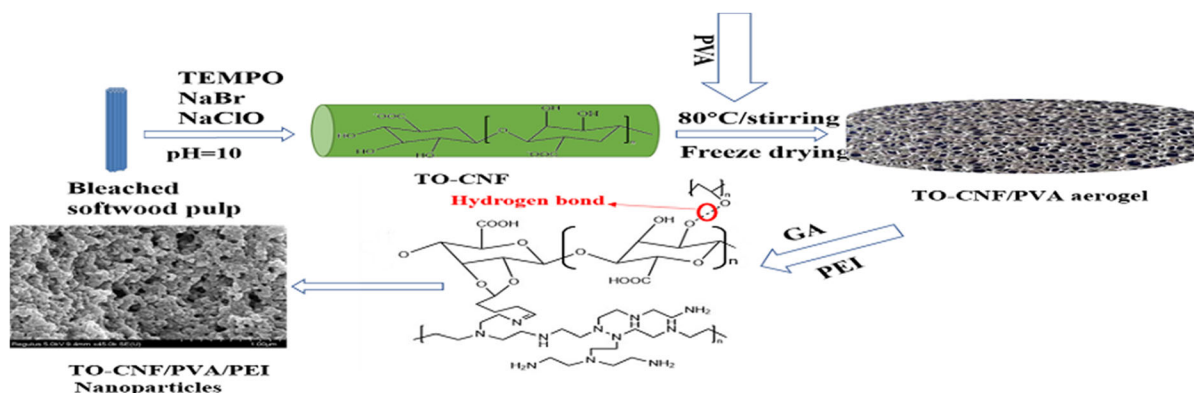
D. Yu  
e-mail: yudongmei197@163.com

R. Si  
e-mail: 2442061985@qq.com

Q. Ding  
e-mail: xianshengding@qlu.edu.cn

R. Li  
e-mail: lrg923@163.com

## Graphic abstract



**Keywords** Cellulose nanofiber · Polyvinyl alcohol · Polyethyleneimine · Copper ion · Adsorption

## Introduction

Nowadays, with the rapid economic growth and industrialization, heavy metal ion pollution (such as copper (Cu) (II), hydrargyrum (Hg) (II), chromium (Cr) (VI), plumbum (Pb) (II) and so on) has been the most serious problem in water environment due to their toxicity and incompatibility (Fu and Wang 2011). Among them, despite being essential for life in minimal amounts, copper easily accumulates in the environment and enters the body through the food chain (Uddin 2017). It has been reported that the heavy metal  $\text{Cu}^{2+}$  usually accumulated in human liver and caused serious anemia and hemolysis (Stern 2010). Therefore, it is necessary to develop green and effective methods to remove  $\text{Cu}^{2+}$  in water.

There are many traditional methods to solve the problems caused by heavy metal ions, such as adsorption, coagulation, membrane separation, oxidation and ion exchange (Wan Ngah and Hanafiah 2008). Among them, adsorption is considered to be one of the most popular strategies for heavy metal ion removal because of the high removal efficiency, flexibility in the design and application of adsorbents, and low cost (Qin et al. 2019b). The adsorbents mainly include activated carbon, clay, biochar and polymers. Recently, nanocellulose based adsorbents become more and more popular as nanocellulose has higher specific surface area, excellent mechanical properties

and good biocompatibility (Du et al. 2016; Jordan et al. 2019).

Tang et al. (2020a) used 3-glycidyloxypropyl trimethoxy silane (GPTMS) as a cross-linking agent to cross-link PEI onto the cellulose nanofibril skeleton and quickly freeze-dried with liquid nitrogen to obtain aerogel beads. Its maximum adsorption capacity for  $\text{Cu}^{2+}$  reached 163.4 mg/g. Zhang et al. (2016) used glutaraldehyde as a cross-linking agent to cross-link PEI onto TEMPO-mediated oxidized cellulose nanofibrils (TOCN) and then freeze-dried to obtain TOCN-PEI adsorbent with a maximum adsorption capacity of 52.32 mg/g for  $\text{Cu}^{2+}$ . Mo et al. (2019) used Trimethylolpropane-tris-(2-methyl-1-aziridine) propionate (TMPTAP) as a cross-linking agent and cross-linked PEI and TO-CNF to obtain TO-CNF/TMPTAP/PEI aerogel. Its maximum adsorption capacity of  $\text{Cu}^{2+}$  could reach 485.44 mg/g.

Poly (vinyl alcohol) (PVA) is an environmentally friendly semi-crystalline, water soluble polymer with good biocompatibility and biodegradability. It has been reported that PVA could be used as environmentally friendly adsorption material due to its excellent characterizations including high oil and chemical resistance and stable in almost all organic solvents (Niu et al. 2018; Zheng et al. 2014). In addition, a higher molecular weight PEI could be degraded to biodegradable polymers (poly (ethylenimine sulfide)) of different molecular weight by using 1,4-butanediol diglycidyl ether (bisepoxide) (Koo et al. 2009, 2010). Furthermore, since PEI has plenty of primary, secondary and tertiary amines on the macromolecular chains, it was usually fabricated hydrogels or aerogels by crosslinking with an aldehyde group for improving

the adsorption capacity (Shao et al. 2017). Therefore, the rich hydroxyl groups on PVA and TO-CNF and the amino group of PEI may form a promising adsorbent under the cross-linking effect of glutaraldehyde.

In this study, we prepared environmentally friendly TO-CNF/PVA/PEI nanoparticles through a freeze-drying method which is beneficial to directly remove water from the nanoparticles with its initial foaming state (Yang et al. 2021). The structures and properties of TO-CNF/PVA/PEI nanoparticles were analyzed by FTIR, SEM, TGA and fully automatic gas adsorption analyzer. The adsorption performance of TO-CNF/PVA/PEI nanoparticles for  $\text{Cu}^{2+}$  was deeply investigated, and its reusability was also being explored.

## Experimental

### Material and methods

**Materials:** Bleached softwood pulp (BSP, Shandong Province, China), 2,2,6,6-Tetramethylpiperidine 1-oxyl (TEMPO, Shanghai, Aladdin.), NaBr (AR grade, Aladdin), sodium hypochlorite solution ( $\text{NaClO}$ , reagent grade, 10–15% chlorine, Aladdin), polyvinyl alcohol (PVA, degree of hydrolysis (87–89%), Sigma-Aldrich), polyethyleneimine (PEI, 70,000 Mw, Macklin), sodium hydroxide ( $\text{NaOH}$ , AR grade, Aladdin), copper nitrate ( $\text{Cu}(\text{NO}_3)_2$ , Beijing, China), glutaraldehyde (GA, 50% in water, Aladdin), hydrochloric acid ( $\text{HCl}$ , 37%, Shandong Province, China).

### Preparation of TEMPO-oxidized cellulose nanofibers (TO-CNF)

The TO-CNF were prepared according to previously reported methods (Qin et al. 2011). Weighed 4 g BSP accurately, dispersed in 400 ml deionized water, then added 0.016 g TEMPO, 0.16 g NaBr and 80 ml 10%  $\text{NaClO}$  into the deionized water. After that, 0.1 M  $\text{HCl}$  was used to adjust the optimal pH value to around 10 which could be maintained by adding 0.5 M  $\text{NaOH}$  solution as the pH value of the solution would gradually decrease with the formation of carboxyl group in the reaction process. Finally, 5 mL ethanol was used to terminate the reaction when the pH value of the solution no longer dropped. After that, the treated wood fibers were rinsed with deionized water

repeatedly until the pH of filter liquid became neutral. The collected fibers were made into 1% suspension with deionized water, and treated with a high-pressure homogenizer at a pressure of 1200 bar for 30 times to obtain TO-CNF.

### Preparation of TO-CNF/PVA aerogel

The PVA solution (12.5 g, 8 wt%), TO-CNF solution (100 g, 1 wt%) were mixed together in a flask under vigorous stirring for 4 h. The weight ratio between the PVA and TO-CNF was 1:1 for the TO-CNF/PVA aerogel (Zheng et al. 2014). At the final stage, the mixture was sonicated in an ultrasonic bath for 1 h under vacuum to remove any bubbles. The TO-CNF/PVA aerogel was obtained using the freeze-drying process described above and was stored in a vacuum oven for further characterization.

### Preparation of TO-CNF/PVA/PEI nanoparticles

Add 2 g TO-CNF/PVA aerogel into 100 ml 10% PEI/methanol (w/v) solution and stir at 30 °C for 24 h. Then with methanol to remove unreacted PEI. Then disperse the precipitate in 100 mL deionized water, then slowly add 4 mL of 25% glutaraldehyde aqueous solution, then adjust the pH to 8 with 0.4 M  $\text{NaOH}$ . Then the system was stirred for one hour to allow the crosslinking between TO-CNF/PVA aerogel and PEI. Finally, the product was separated and washed thoroughly with deionized water and then freeze-dried to obtain TO-CNF/PVA/PEI nanoparticle adsorbent.

## Characterization

### FTIR

Fourier transform infrared spectroscopy (IR Prestige21, Shimadzu Corporation) spectra were obtained using the Alpha infrared spectrometer with a scanning number of 32 from 250 to 4250  $\text{cm}^{-1}$ .

### SEM

Scanning electron microscope (Regulus 8220, Japan) was used to characterize the morphology of materials. All the specimens were coated with Au before observation.

## TGA

Thermogravimetric analysis (TGA) was conducted with a synchronous thermal analyzer (STA449, USA) test. Samples were heated at a constant heating rate of 10 °C/ min, from room temperature (RT) to 650 °C, under inert (N<sub>2</sub>) atmosphere.

## BET

The specific surface areas were measured by the Brunauer–Emmett–Teller (BET) method based on N<sub>2</sub> adsorption. The determinations were carried out from freeze-dried samples with an analyzer (Micromeritics, USA). Prior to testing, the samples should be degassed at 120 °C for 4 h.

## Adsorption experiments

Adsorption experiments were conducted by the batch method to examine the sorption kinetics and isotherm of Cu<sup>2+</sup> ions by TO-CNF/PVA/PEI nanoparticles. A mount of adsorbents (0.05, 0.1 g) and metal ion solution (50 mL) were added into a 100 mL flask. 0.05 g of adsorbent was used to investigate the optimal adsorption pH. The effect of initial pH values in the range of 2–6 was investigated, where the pH of the Cu<sup>2+</sup> solution was controlled by adding 1 M HCl and 1 M NaOH solutions. Then the flask was placed in Temersionoxcillator registration (Noki) at room temperature to reach the adsorption equilibrium. 0.1 g adsorbent for removal rate study, 0.1 g adsorbent for kinetics study, the effect of contact time in the range between 0 and 2 h was investigated at 25 °C. 0.1 g adsorbent for the adsorption isotherm study, the initial Cu<sup>2+</sup> concentrations were varied from 20 to 400 mg/L. Residual concentration of Cu<sup>2+</sup> were measured by flame atomization atomic absorption spectrometry (AAS, GGX-600, China), the equilibrium adsorption capacity (q<sub>e</sub>, mg/g) was analyzed according to (Eq. (1)) (Anirudhan et al. 2019).

$$q_e = \frac{(C_0 - C_e) * V}{m} \quad (1)$$

where C<sub>0</sub> is the initial concentration of Cu<sup>2+</sup> (mg/L) and C<sub>e</sub> is the concentration of Cu<sup>2+</sup> at equilibrium time (Li et al. 2018); V (mL) is the volume of the solution and m (mg) is the adsorbent dose.

## Data analysis

The adsorption kinetic data of the Cu<sup>2+</sup> onto TO-CNF/PVA/PEI nanoparticles were simulated with the pseudo-first-, second-order kinetic, Intra-particle diffusion model and Elovich equation, which were expressed as (Eqs. (2), (3), (4) and (5))

$$\ln(Q_0 - Q_t) = \ln Q_0 - K_1 t \quad (2)$$

$$\frac{t}{Q_t} = \frac{1}{k_2 Q_0^2} + \frac{t}{Q_0} \quad (3)$$

$$Q_t = k_i t^{0.5} + C \quad (4)$$

$$Q_t = A + k_e \ln t \quad (5)$$

where Q<sub>t</sub> is the adsorption capacity after time t and Q<sub>0</sub> is the saturated adsorption capacity of Cu<sup>2+</sup>; k<sub>1</sub> and k<sub>2</sub> are the rate constants of the pseudo first-order and second-order kinetics respectively; k<sub>i</sub> and C are the constants of the Intra-particle diffusion model; k<sub>e</sub> and A are the constants of the Elovich equation.

The adsorption isotherms of Cu<sup>2+</sup> adsorption by TO-CNF/PVA/PEI nanoparticles. The Langmuir and Freundlich adsorption isotherm models were employed to analyze the experimental data, which were represented as (Eqs. (6) and (7))

$$\frac{C_e}{Q_e} = \frac{C_e}{Q_m} + \frac{1}{Q_m b} \quad (6)$$

$$\lg Q_e = \lg K_f + \frac{1}{n} \lg C_e \quad (7)$$

where Q<sub>e</sub> (mg/g) is the equilibrium adsorption capacity, C<sub>e</sub> (mg/L) is the metal ion solution concentration at equilibrium, Q<sub>m</sub> (mg/g) is the maximum adsorption capacity and b is the Langmuir adsorption constant related to adsorption energy, K<sub>f</sub> and n are the Freundlich adsorption constants which indicate the capacity and intensity of the adsorption, respectively.

## Desorption experiments

The 100 mg TO-CNF/PVA/PEI nanoparticles adsorbed with Cu<sup>2+</sup> were dispersed in 1 M HCl solution and stirred at room temperature for 1 h to remove Cu<sup>2+</sup> ions. Then, the nanoparticles were repeatedly submerged into deionized water to remove the excess acid until the pH value of solution was equal

to around 7, and the nanoparticles were dried for the next adsorption process.

## Results and discussions

### Crosslinking types in TO-CNF/PVA aerogel and TO-CNF/PVA/PEI nanoparticles

It is clear that bleached softwood pulp has absorption peaks at  $3400\text{ cm}^{-1}$ ,  $1430\text{ cm}^{-1}$ ,  $1370\text{ cm}^{-1}$ ,  $1322\text{ cm}^{-1}$  and  $897\text{ cm}^{-1}$  (Fig. 1), which are O–H group stretching vibration, C–H scissoring vibration, C–H bending vibration, O–H in -plane vibration and C–H deformation vibration of cellulose, respectively (Sirvio et al. 2015; Tarchoun et al. 2019). It can be observed that TO-CNF appears an intense peak in  $1606\text{ cm}^{-1}$ , which was assigned to the characteristic peak of the carbonyl of the carboxylic acid group.

Compared with TO-CNF, an absorption peak belonging to PVA appeared at  $850\text{ cm}^{-1}$  of TO-CNF/PVA aerogel, it may be caused by the formation of intermolecular hydrogen bonds (Takeno et al. 2020). For TO-CNF/PVA/PEI nanoparticles, the peak in the  $1600\text{--}1800\text{ cm}^{-1}$  region appeared to be the overlap the three individual peaks, which belonged to N–H bending vibration ( $1615\text{ cm}^{-1}$ ), C=O stretching vibration for  $\text{--COO--}$  ( $1660\text{ cm}^{-1}$ ) and for  $\text{--COOH}$  ( $1713\text{ cm}^{-1}$ ), respectively. The vibration shifted to a higher wavenumber due to the hydrogen bonds existing between amino and carboxyl groups. The adsorption peak at about  $1660\text{ cm}^{-1}$  should also be

contributed from stretching C=N groups, which was formed in the glutaraldehyde crosslinking process. In addition, at  $2923\text{ cm}^{-1}$  and  $2848\text{ cm}^{-1}$  as early as  $\text{--CH}_2\text{--}$  stretching vibrations could also prove that PEI likely assembled into the TO-CNF/PVA aerogel (Tang et al. 2020b).

### Morphological analysis of TO-CNF, TO-CNF/PVA aerogel and TO-CNF/PVA/PEI nanoparticles

The morphology and structure of BSP, TO-CNF suspension is dispersed on mica flakes, TO-CNF aerogel, TO-CNF/PVA aerogel and TO-CNF/PVA/PEI nanoparticles were examined by SEM (Fig. 2.) The overall and local fiber morphology of BSP was observed at 1 K and 60 K, respectively. It can be clearly seen that the diameter of cellulose fiber was about 20–30 microns, and the length could reach vertical microns. SEM results show that there are some pores with diameter of 10–20 nm on the surface of cellulose. The TO-CNF obtained by homogenizing after TEMPO oxidation had a diameter between 10 and 50 nm and a length of a few microns. It can be seen that TO-CNF had an excellent aspect ratio, which could have a positive effect on subsequent adsorption (Garba et al. 2020). The morphology of TO-CNF aerogel and TO-CNF/PVA aerogel were all observed at 0.03 K, and it was found that the morphology of the two aerogels was completely different, the surface of TO-CNF aerogel was honeycomb structure, however, the surface of TO-CNF/PVA aerogels was porous. The TO-CNF/PVA aerogel had a porous network structure on the surface, which would provide a larger area for the cross-linking of PEI. With the action of glutaraldehyde cross-linking agent, PEI was cross-linked on TO-CNF/PVA aerogel, this resulted in an obvious change in the morphology of TO-CNF/PVA/PEI compared with TO-CNF/PVA aerogel. The surface of TO-CNF/PVA/PEI becomes denser and many granular nanoparticles appeared. These phenomena indicated that PEI played a great role in changing the surface morphology during the cross-linking process. Nano Measurer Software was used to count the particle size distribution of TO-CNF/PVA/PEI nanoparticles. According to the calculation, the particle size of TO-CNF/PVA/PEI nanoparticles was mainly distributed between 40 and 80 nm, accounting for 83% of the total.

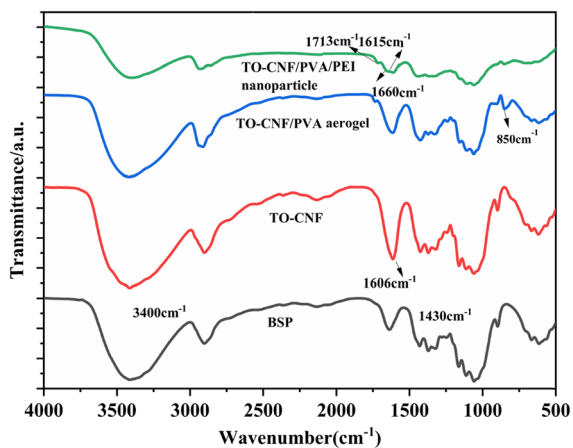


**Fig. 1** FTIR analysis of BSP, TO-CNF, TO-CNF/PVA aerogel, TO-CNF/PVA/PEI nanoparticles

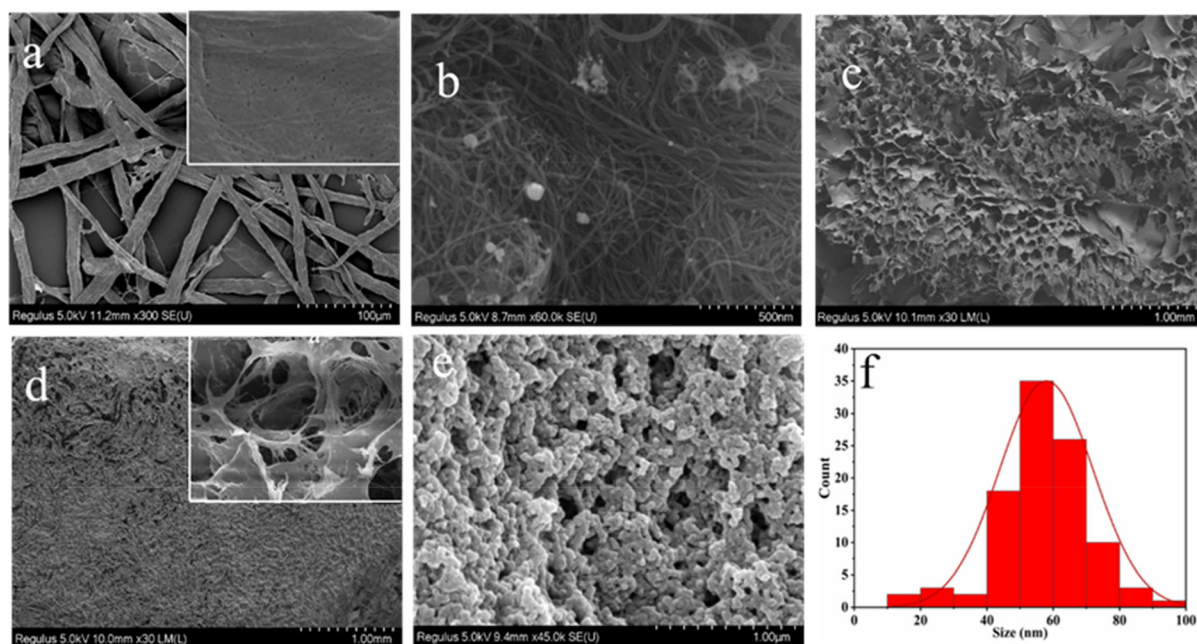


**Fig. 2** SEM images of **a** BSP, **b** TO-CNF, **c** TO-CNF aerogel, **d** TO-CNF/PVA aerogel, **e** TO-CNF/PVA/PEI nanoparticles, **f** Particle size distribution of TO-CNF/PVA/PEI nanoparticles

#### Thermal stability of TO-CNF, TO-CNF/PVA aerogel and TO-CNF/PVA/PEI nanoparticles

The thermal degradation profiles of BSP, TO-CNF, TO-CNF/PVA aerogel and TO-CNF/PVA/PEI nanoparticles were assessed by thermogravimetric analysis (TGA) under nitrogen atmosphere from RT (room temperature) to 650 °C (Fig. 3a). During the process from RT to 100 °C, due to the loss of water, the three substances have a slight quality degradation (not more than 2%) (Eun et al. 2020; Rani et al. 2014). BSP loses the fastest weight in 280–399 °C, which was the main stage of cellulose pyrolysis. Within this range, BSP was pyrolyzed into small molecular gases and condensable volatiles of macromolecules, resulting in significant weight loss, and its weight loss rate reached its maximum at about 384.9 °C. The maximum degradation temperature of TO-CNF is 320 °C (about 50% loss), which is used for the pyrolysis of the cellulose skeleton (Yao et al. 2017). At the end of the analysis, the mass percentage of TO-CNFs pyrolysis residue was 26%. The TO-CNF/PVA aerogel showed its first decline at 221.8 °C, and the maximum degradation temperature (loss of ca. 40%) appears at about 324.7 °C. TO-CNF/PVA/PEI nanoparticles have their first degradation at 216.4 °C, and the

maximum degradation temperature is 327.5 °C (loss of ca. 52%). At the end of the analysis, the remaining TO-CNF/PVA aerogel and TO-CNF/PVA/PEI nanoparticles were 31% and 16%, respectively. The thermal stability of the adsorbents up to 205 °C could be a valuable asset in the industrial sector context where the effluents could be warm or hot (Silva et al. 2020) (Table 1).

#### Specific surface area of TO-CNF, TO-CNF/PVA aerogel and TO-CNF/PVA/PEI nanoparticles

Figure 3b shows the N<sub>2</sub> adsorption–desorption curve of the sample at a temperature of 77 K. The curve of TO-CNF/PVA/PEI nanoparticles shown in the figure is type 4, which also verifies that the nanoparticles have a mesoporous structure (Wang et al. 2019). As seen in Table 2, the BET specific surface area of TO-CNF aerogel and TO-CNF/PVA aerogel were 35.52 m<sup>2</sup>/g and 56.37 m<sup>2</sup>/g, respectively. After PEI modification, the BET specific surface area of TO-CNF/PVA/PEI nanoparticles became 22.93 m<sup>2</sup>/g, which indicated that PEI was successfully assembled into the TO-CNF/PVA aerogel.

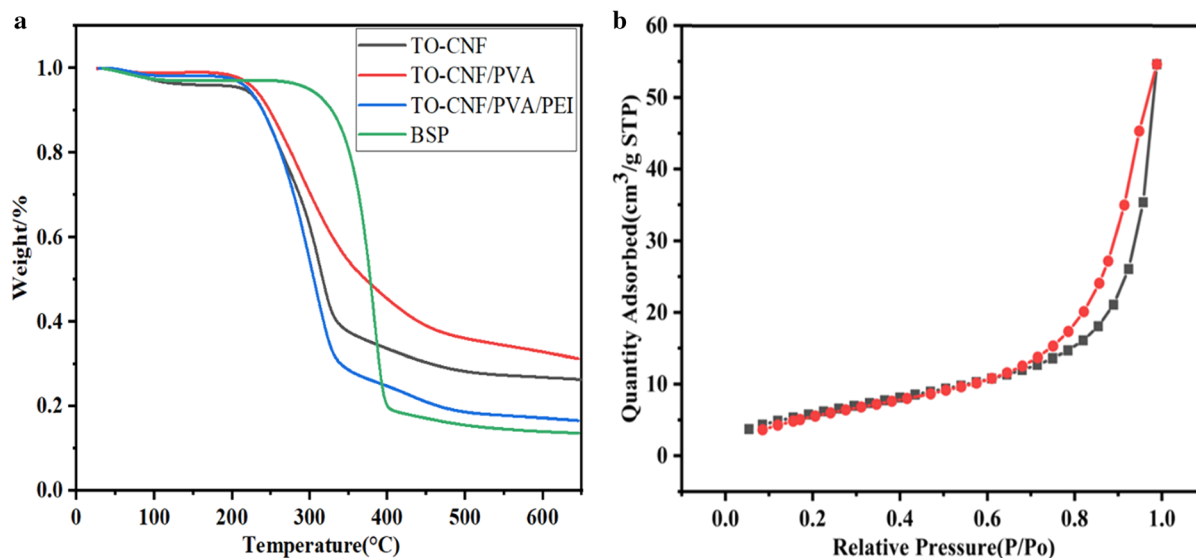


**Fig. 3** a TGA for BSP, TO-CNF, TO-CNF/PVA aerogel, TO-CNF/PVA/PEI nanoparticles. b Adsorption–desorption isotherm and pore size distribution of TO-CNF/PVA/PEI nanoparticles at 77 K

**Table 1** Thermal stability parameters of BSP, TO-CNF, TO-CNF/PVA aerogel, TO-CNF/PVA/PEI nanoparticles

Sample	BSP	TO-CNF	TO-CNF/PVA	TO-CNF/PVA/PEI
$T_0$ (°C)	269.8	168.2	177.6	194.9
$T_{5\%}$ (°C)	294.1	207.1	221.8	216.4
$T_{max}$ (°C)	384.9	312.7	324.7	327.5

<sup>a</sup> $T_0$ ,  $T_{5\%}$ ,  $T_{max}$  were calculated from TGA curves

**Table 2** Specific surface area and average pore size of TO-CNF, TO-CNF/PVA aerogel, TO-CNF/PVA/PEI nanoparticles

Sample	BET surface area (m <sup>2</sup> /g)	Langmuir surface area (m <sup>2</sup> /g)	Pore size (Å)
TO-CNF/PVA Aerogel	56.37	307.8	55.15
TO-CNF/PVA/PEI nanoparticles	22.93	183.6	85.67

### Effect of pH on Cu<sup>2+</sup> adsorption

The initial pH value of the copper solution had a crucial influence on the absorption performance of the adsorbent since it determined the form of the copper ion species and the electrostatic repulsion between the adsorbent and Cu<sup>2+</sup> ions. Due to the presence of amino groups in TO-CNF/PVA/PEI, the surface charge would change with the change of pH, thereby affecting the adsorption capacity. In addition, when the pH exceeded 6.5, Cu<sup>2+</sup> ions could be converted to Cu(OH)<sub>2</sub> precipitation (Shao et al. 2017). As shown in the Fig. 4a, the adsorption capacity of TO-CNF/

PVA/PEI nanoparticles was measured under five different pH values of 2, 3, 4, 5, 6. The adsorption capacity of TO-CNF/PVA/PEI nanoparticles for Cu<sup>2+</sup> increased with the increase of pH value. Due to the protonation of the amino group, it exhibits a lower adsorption capacity at a lower pH value. At low pHs, the amino group was protonated to achieve the goal of removing Cu<sup>2+</sup>. This was possibly due to electrostatic attraction between the carboxyl group and Cu<sup>2+</sup>. The adsorption capacity could reach the maximum at pH 6, so the optimal adsorption performance of TO-CNF / PVA/PEI nanoparticles could be characterized at this pH value.

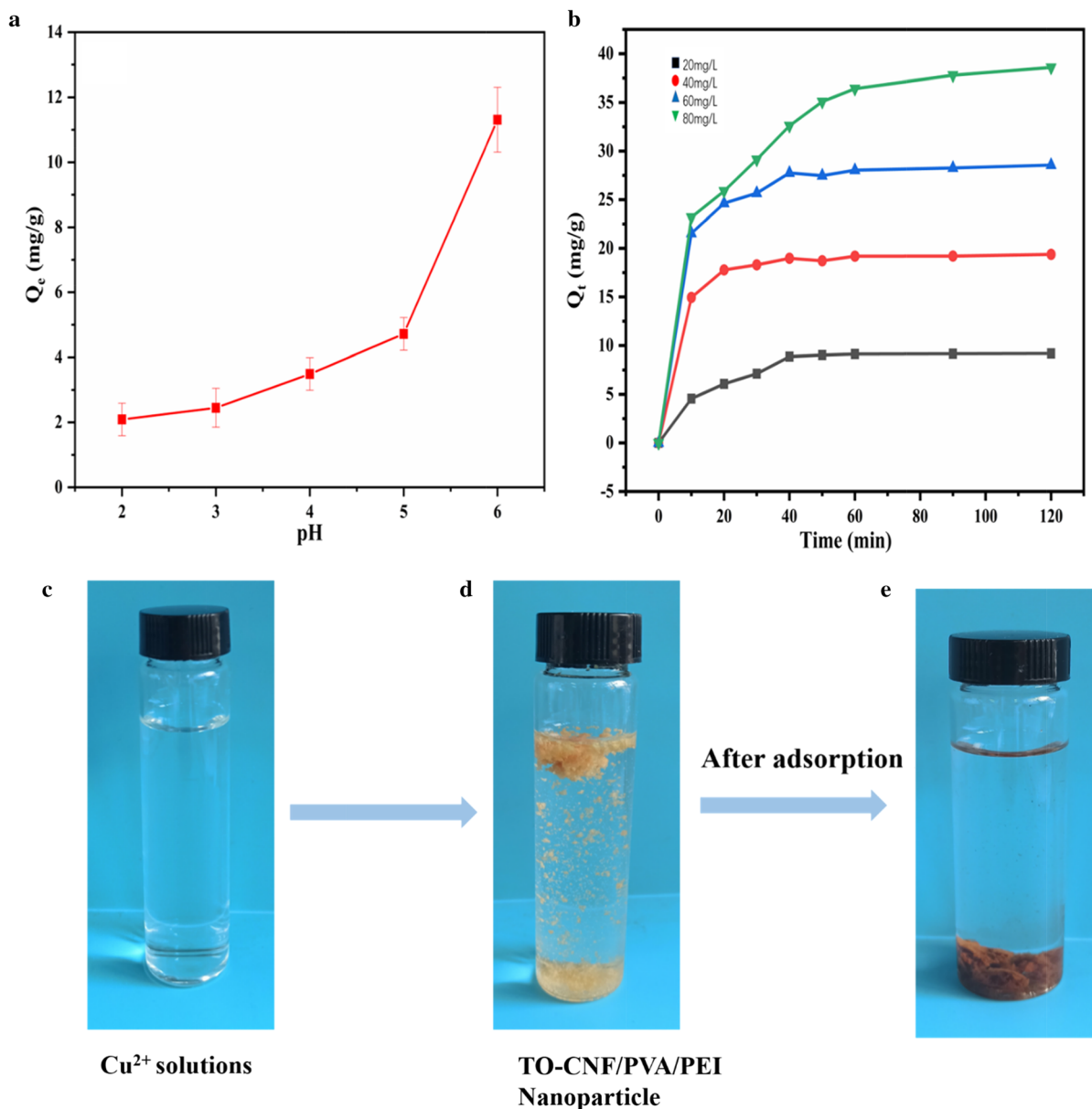


**Fig. 4** **a** Effect of initial pH on the adsorption of  $\text{Cu}^{2+}$  onto TO-CNF/PVA/PEI nanoparticles. **b** Contact time versus removal capacity of TO-CNF/PVA/PEI nanoparticles for  $\text{Cu}^{2+}$ . (**c**–

**e**) Photographs of the TO-CNF/PVA/PEI nanoparticles being inserted into the  $\text{Cu}^{2+}$ -contaminated deionized water

#### Adsorption kinetics

As shown in the Fig. 4b, at the beginning, the adsorption capacity of TO-CNF/PVA/PEI nanoparticles for  $\text{Cu}^{2+}$  increased rapidly with increased adsorption time from 0 to 60 min, and nearly reached adsorption equilibrium after 60 min, which was likely due to the reduction of effective adsorption sites.

Figure 4c–e showed digital photographs of the  $\text{Cu}^{2+}$  adsorption in 20 mg/L of the adsorbent. As seen, the color of TO-CNF/PVA/PEI nanoparticles changed obviously after adsorption.

Usually, various linear models were used to simulate the adsorption kinetics in heavy metal removal field due to their clear and simple characteristics (Qin et al. 2019a; Tang et al. 2020b). The fitting kinetic



**Table 3** The fitting parameters of adsorption kinetics of Cu<sup>2+</sup>

Models	Parameters	Concentration (mg/L)			
		20	40	60	80
Pseudo-first-order	$k_1/(\text{min}^{-1})$	-0.07115	-0.05069	-0.04057	-0.03465
	$R^2$	0.9159	0.9102	0.9006	0.9677
Pseudo-second-order	$k_2/(\text{g}/\text{mg} \cdot \text{min})$	0.1002	0.05098	0.03394	0.02432
	$R^2$	0.9906	0.9994	0.9997	0.9971
Elovich equation	$k_e$	2.047	1.640	2.849	6.935
	C	0.3018	12.25	15.92	6.608
	$R^2$	0.8617	0.8065	0.9048	0.9594
Intra-particle diffusion	$k_i$	0.5702	0.4411	0.8220	2.020
	A	3.969	15.39	20.87	18.39
	$R^2$	0.6922	0.5616	0.7609	0.8709

parameters from four models were summarized in Table 3. and Fig. 5. At different concentrations, the time to reach adsorption equilibrium is the same,

therefore, the higher the concentration, the higher the adsorption rate. The results show that  $k_1$  increases and  $k_2$  decreases as the rate increases,  $k_i$  and  $k_e$  show a

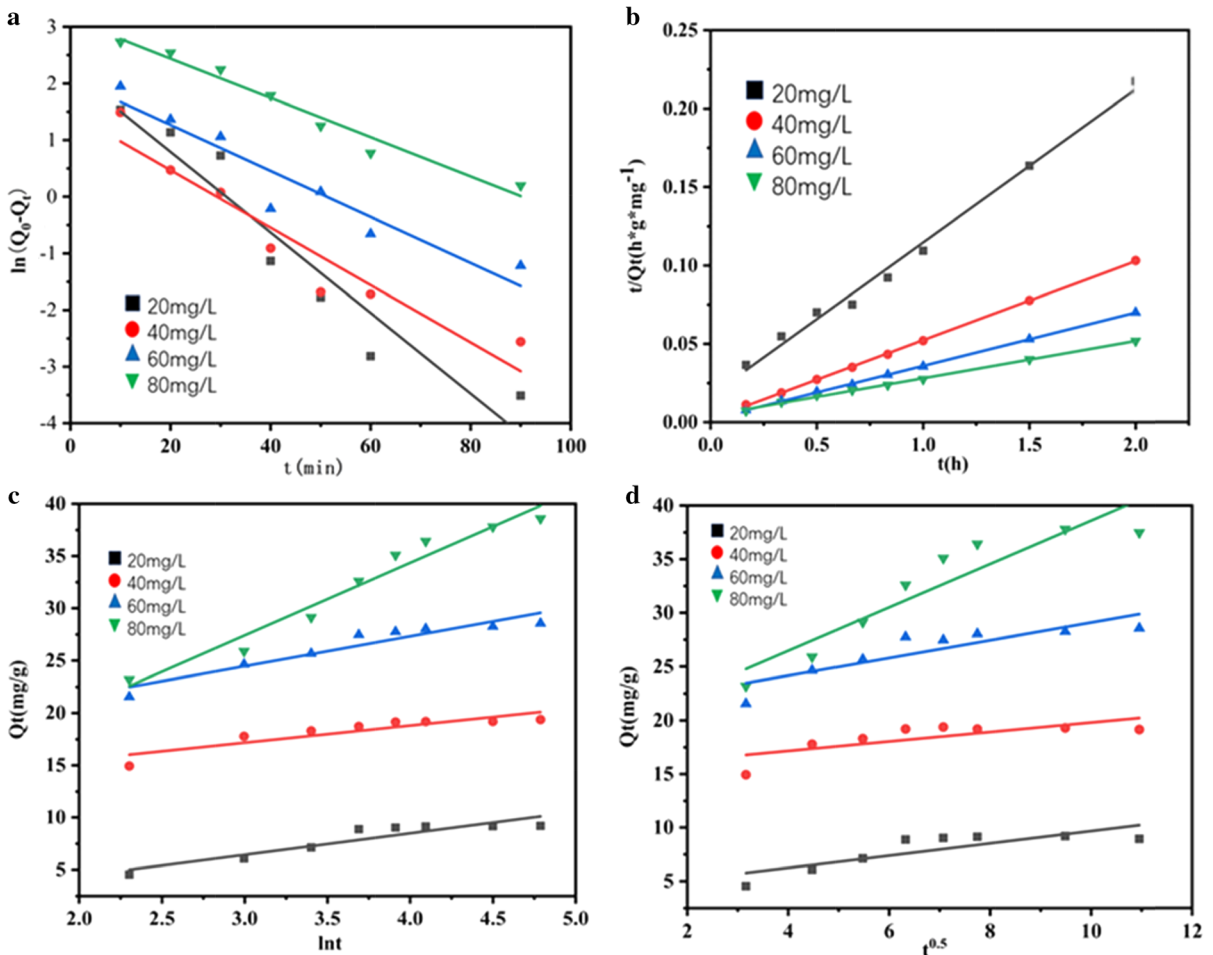


**Fig. 5** a Plots of Pseudo-first-order, b Pseudo-second-order, c Elovich, d Intra-particle diffusion models of 20, 40, 60, 80 mg/L

similar change pattern, decreasing first and then increasing with the increase of concentration. At four different concentrations, the correlation coefficient ( $R^2$ 's) of the Pseudo-second-order model is all above 0.99. However, for the Pseudo-first-order model, the  $R^2$ 's is between 0.9006 and 0.9677. The fitting results of the Intra-particle diffusion model are not very good, and the  $R^2$ 's of the four concentrations are all less than 0.87. For the fitting results of Elovich equation, the  $R^2$ 's of the four concentrations are between 0.8065 and 0.9594. Therefore, the Pseudo-second-order model is considered to be the most suitable data for experimental results. This result indicated that  $\text{Cu}^{2+}$  adsorption was dominated by chemical adsorption (Lei et al. 2020). Functional groups such as hydroxyl and amino groups in TO-CNF/PVA/PEI nanoparticles provide adsorption sites for chemical adsorption. Large specific surface area would provide more opportunities for the adsorption of heavy metal ions.

#### Adsorption isotherms

The adsorption isotherm parameters and graphics were displayed in Fig. 6 and Table 4, respectively. The higher correlation coefficient of the Langmuir model illustrated that the experimental data fitted the Langmuir model ( $R^2 > 0.99$ ) better than the Freundlich model. It was proved that the adsorption process was monolayer adsorption according to the assumptions of the Langmuir model (Li et al. 2018). This speculation suggested that a homogeneous monolayer was likely

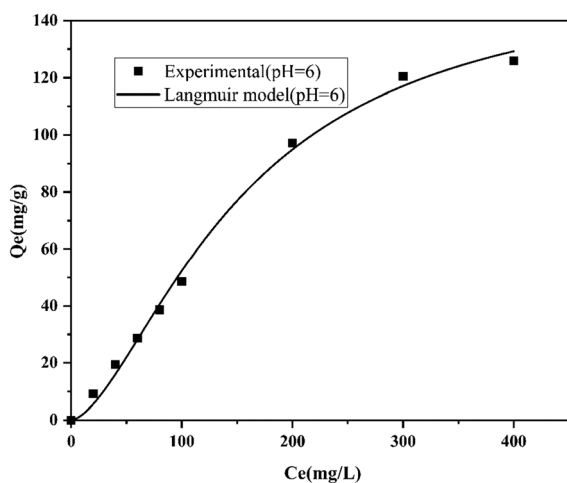


**Fig. 6** Isotherm models of  $\text{Cu}^{2+}$  adsorption by TO-CNF/PVA/PEI nanoparticles at pH 6

formed on TO-CNF/PVA/PEI nanoparticles when  $\text{Cu}^{2+}$  was adsorbed. This was likely due to the electrostatic attraction between the carboxyl groups and the divalent metal ions, as well as the chelation between the amine groups and the metal ions. According to the Langmuir parameter, the theoretical maximum adsorbed amounts of  $\text{Cu}^{2+}$  was 156.8 mg/g.

#### Desorption ability of TO-CNF/PVA/PEI nanoparticles

In addition to desired removal rate, ideal environmental remediation materials should possess excellent regeneration and recyclability. It was obvious that the  $\text{Cu}^{2+}$  removal rate of TO-CNF/PVA/PEI nanoparticles retained 80% after three adsorption–desorption cycles (Fig. 7). The removal rate was decreased slightly with the cycle time, which was due to the decrease of effective adsorption sites in TO-CNF/PVA/PEI nanoparticles. There were two reasons to result in the reduction of removal rate. One of that was unable to desorb completely due to  $\text{Cu}^{2+}$  combined with some active sites of TO-CNF/PVA/PEI

**Table 4** Isotherms parameters for the adsorption of  $\text{Cu}^{2+}$

	Langmuir Model			Freundlich Model		
	Qe (mg/g)	B	$R^2$	1/n	$K_f$	$R^2$
$\text{Cu}^{2+}$	156.8	0.0002	0.9950	0.16	49.89	0.96

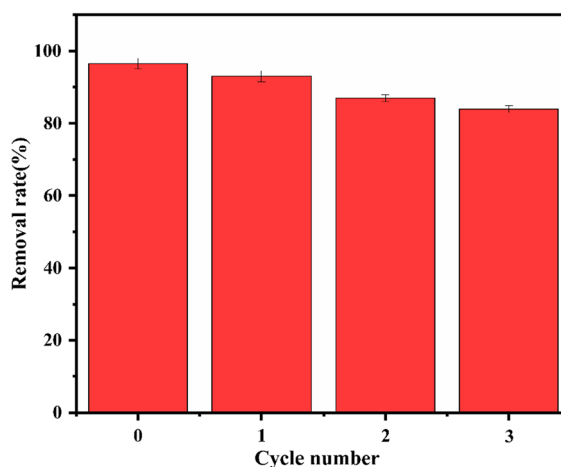


**Fig. 7** Recycling performance of TO-CNF/PVA/PEI nanoparticles for  $\text{Cu}^{2+}$  adsorption

**Table 5** Comparison of adsorption capacity of different adsorption materials

Adsorbent	Adsorption equilibrium	Adsorption capacity (mg/g)	Cycles times	Ref
DNFCs	8 h	29.52	/	(Lei et al. 2019)
CMCNF-2.7	3 min	115.3	/	(Qin et al. 2019a)
POCNF-PEI	1500 min	74.2	4	(Tang et al. 2020b)
TOCN-PEI	25 h	52.32	4	(Zhang et al. 2016)
TO-CNF/PVA/PEI nanoparticles	1 h	156.8	3	This work

nanoparticles during the desorption process. Due to desorption under acidic conditions, a few amine groups may be protonated, thus leading to the occurrence of this phenomenon (Tang et al. 2020b).

#### Comparison with reported studies

The final adsorption properties of TO-CNF/PVA/PEI nanoparticles were evaluated and presented in Table 5 for comparison with reported data. The TO-CNF/PVA/PEI nanoparticles reached adsorption equilibrium within one hour, far better than the 2,3-dialdehyde nano-fibrillated celluloses (DNFCs) (Lei et al. 2019), pomelo cellulose nanofibers-PEI (POCNF-PEI) (Tang et al. 2020b) and TOCN-PEI (Zhang et al. 2016). The adsorption capacity of TO-CNF/PVA/PEI nanoparticles reached 156.82 mg/g. It was far higher than that of other CNF-based adsorbents. It was clear that the removal rate could still retain 80% after three cycles. This indicated that TO-CNF/PVA/PEI nanoparticles was an excellent adsorbent, and could successfully be applied in practical application in the near future.

#### Conclusion

To improve the removal rate and adsorption capability of TO-CNF based adsorbents for  $\text{Cu}^{2+}$ , we introduce a novel and green approach to assemble TO-CNF/PVA/PEI nanoparticles, which reaches fast adsorption of  $\text{Cu}^{2+}$ . Its adsorption for  $\text{Cu}^{2+}$  is very consistent with the pseudo-second-order model among four kinds of adsorption models. It is evident that the chemical adsorption is the main adsorption mechanism when the TO-CNF based adsorbent is carried out to remove  $\text{Cu}^{2+}$  in water. We can assemble the environmentally

friendly and effective TO-CNF based adsorbents for the removal of  $\text{Cu}^{2+}$  by doping new chemical agents and controlling the structure in the near future. Overall, this study not only reveals adsorption mechanism of TO-CNF/PVA/PEI nanoparticles for  $\text{Cu}^{2+}$  removal, but also provides a promising pathway to regulate the TO-CNF based adsorbents for the removal of the other heavy metal ions in water.

**Authors' contribution** All authors contributed as the main contributors of this work. All authors performed the literature search and analysis. All authors had drafted, revised the work and approved the final paper.

**Funding** This article was financially supported by the National Key R&D Program of China (2017YFB0307900) and the Foundation (No. ZZ20200107) of State Key Laboratory of Biobased Material and Green Papermaking, Qilu University of Technology, Shandong Academy of Sciences.

#### Declarations

**Conflict of interest** The authors declare that they have no conflict of interest.

**Ethical approval** This article does not contain any studies with human participants or animals performed by any of the authors.

#### References

- Anirudhan TS, Shainy F, Deepa JR (2019) Effective removal of Cobalt(II) ions from aqueous solutions and nuclear industry wastewater using sulfhydryl and carboxyl functionalised magnetite nanocellulose composite: batch adsorption studies. *Chem Ecol* 35:235–255. <https://doi.org/10.1080/02757540.2018.1532999>
- Du HS et al (2016) Preparation and characterization of thermally stable cellulose nanocrystals via a sustainable approach of  $\text{FeCl}_3$ -catalyzed formic acid hydrolysis. *Cellulose*

- 23:2389–2407. <https://doi.org/10.1007/s10570-016-0963-5>
- Eun S, Hong HJ, Kim H, Jeong HS, Kim S, Jung J, Ryu J (2020) Prussian blue-embedded carboxymethyl cellulose nanofibril membranes for removing radioactive cesium from aqueous solution. *Carbohydr Polym*. <https://doi.org/10.1016/j.carbpol.2020.115984>
- Fu F, Wang Q (2011) Removal of heavy metal ions from wastewaters: a review. *J Environ Manage* 92:407–418. <https://doi.org/10.1016/j.jenvman.2010.11.011>
- Garba ZN, Lawan I, Zhou W, Zhang M, Wang L, Yuan Z (2020) Microcrystalline cellulose (MCC) based materials as emerging adsorbents for the removal of dyes and heavy metals - A review. *Sci Total Environ*. <https://doi.org/10.1016/j.scitotenv.2019.135070>
- Jordan JH, Easson MW, Condon BD (2019) Alkali hydrolysis of sulfated cellulose nanocrystals: optimization of reaction conditions and tailored surface charge. *Nanomaterials* 9:15. <https://doi.org/10.3390/nano9091232>
- Koo H, Jin G, Kang H, Lee Y, Nam HY, Jang H, Park JS (2009) A new biodegradable crosslinked polyethylene oxide sulfide (PEOS) hydrogel for controlled drug release. *Int J Pharm* 374:58–65. <https://doi.org/10.1016/j.ijpharm.2009.03.010>
- Koo H, Jin GW, Kang H, Lee Y, Nam K, Bai CZ, Park JS (2010) Biodegradable branched poly(ethyleneimine sulfide) for gene delivery. *Biomaterials* 31:988–997. <https://doi.org/10.1016/j.biomaterials.2009.10.004>
- Lei Z, Gao W, Zeng J, Wang B, Xu J (2019) The mechanism of Cu (II) adsorption onto 2,3-dialdehyde nano-fibrillated celluloses. *Carbohydr Polym*. <https://doi.org/10.1016/j.carbpol.2019.115631>
- Lei ZH, Gao WH, Zeng JS, Wang B, Xu J (2020) The mechanism of Cu (II) adsorption onto 2,3-dialdehyde nano-fibrillated celluloses. *Carbohydr Polym* 230:8. <https://doi.org/10.1016/j.carbpol.2019.115631>
- Li et al (2018) Shape memory aerogels from nanocellulose and polyethyleneimine as a novel adsorbent for removal of Cu(II) and Pb(II). *Carbohydr Polym* 196:376–384. <https://doi.org/10.1016/j.carbpol.2018.05.015>
- Mo L (2019) 3D multi-wall perforated nanocellulose-based polyethyleneimine aerogels for ultrahigh efficient and reversible removal of Cu(2+) ions from water. *Chem Eng J*. <https://doi.org/10.1016/j.cej.2019.122157>
- Niu X, Liu YT, Fang GG, Huang CB, Rojas OJ, Pan H (2018) Highly transparent, strong, and flexible films with modified cellulose nanofiber bearing UV shielding property. *Biomacromol* 19:4565–4575. <https://doi.org/10.1021/acs.biomac.8b01252>
- Qin ZY, Tong GL, Chin YCF, Zhou JC (2011) Preparation of ultrasonic-assisted high carboxylate content cellulose nanocrystals by TEMPO oxidation. *Bioresources* 6:1136–1146
- Qin FM et al (2019) Efficient removal of Cu<sup>2+</sup> in water by carboxymethylated cellulose nanofibrils: performance and mechanism. *Biomacromolecules* 20:4466–4475. <https://doi.org/10.1021/acs.biomac.9b01198>
- Qin H, Hu T, Zhai Y, Lu N, Aliyeva J (2019) The improved methods of heavy metals removal by biosorbents: a review. *Environ Pollut*. <https://doi.org/10.1016/j.envpol.2019.113777>
- Rani MSA, Rudhziah S, Ahmad A, Mohamed NS (2014) Biopolymer electrolyte based on derivatives of cellulose from Kenaf Bast fiber. *Polymers* 6:2371–2385. <https://doi.org/10.3390/polym6092371>
- Shao et al (2017) Soy protein-based polyethylenimine hydrogel and its high selectivity for copper ion removal in wastewater treatment. *J Mater Chem A* 5:4163–4171. <https://doi.org/10.1039/c6ta10814h>
- Silva NHCS, Figueira P, Fabre E, Pinto RJB, Freire CSR (2020) Dual nanofibrillar-based bio-sorbent films composed of nanocellulose and lysozyme nanofibrils for mercury removal from spring waters. *Carbohydr Polym* 238:116210. <https://doi.org/10.1016/j.carbpol.2020.116210>
- Sirvio JA, Visanko A, Liimatainen H (2015) Deep eutectic solvent system based on choline chloride-urea as a pre-treatment for nanofibrillation of wood cellulose. *Green Chem* 17:3401–3406. <https://doi.org/10.1039/c5gc00398a>
- Stern BR (2010) Essentiality and toxicity in copper health risk assessment: overview, update and regulatory considerations. *J Toxicol Env Health Part A* 73:114–127. <https://doi.org/10.1080/15287390903337100>
- Takeo H, Inoguchi H, Hsieh WC (2020) Mechanical and structural properties of cellulose nanofiber/poly(vinyl alcohol) hydrogels cross-linked by a freezing/thawing method and borax. *Cellulose* 27:4373–4387. <https://doi.org/10.1007/s10570-020-03083-z>
- Tang CX, Brodie P, Li YZ, Grishkewich NJ, Brunsting M, Tam KC (2020) Shape recoverable and mechanically robust cellulose aerogel beads for efficient removal of copper ions. *Chem Eng J* 392:11. <https://doi.org/10.1016/j.cej.2020.124821>
- Tang F et al (2020) Green acid-free hydrolysis of wasted pomelo peel to produce carboxylated cellulose nanofibers with super absorption/flocculation ability for environmental remediation materials. *Chem Eng J*. <https://doi.org/10.1016/j.cej.2020.125070>
- Tarchoun AF, Trache D, Klapotke TM, Derradji M, Bessa W (2019) Ecofriendly isolation and characterization of microcrystalline cellulose from giant reed using various acidic media. *Cellulose* 26:7635–7651. <https://doi.org/10.1007/s10570-019-02672-x>
- Uddin MK (2017) A review on the adsorption of heavy metals by clay minerals, with special focus on the past decade. *Chem Eng J* 308:438–462. <https://doi.org/10.1016/j.cej.2016.09.029>
- Wan Ngah WS, Hanafiah MA (2008) Removal of heavy metal ions from wastewater by chemically modified plant wastes as adsorbents: a review. *Bioresour Technol* 99:3935–3948. <https://doi.org/10.1016/j.biortech.2007.06.011>
- Wang X et al (2019) Facile fabrication of superhydrophobic and eco-friendly polylactic acid foam for oil-water separation via skin-peeling. *ACS Appl Mater Inter*. <https://doi.org/10.1021/acsami.9b02285>
- Yang JJ, Wang ZJ, Zhao G (2021) Investigation into output force performance of an ionic polymer artificial muscle based on freeze-drying process. *Sens Actuator A-Phys* 321:9. <https://doi.org/10.1016/j.sna.2020.112427>
- Yao QF, Fan BT, Xiong Y, Jin CD, Sun QF, Sheng CM (2017) 3D assembly based on 2D structure of cellulose nanofibril/graphene oxide hybrid aerogel for adsorptive removal of

- antibiotics in water. *Sci Rep* 7:13. <https://doi.org/10.1038/srep45914>
- Zhang N, Zang G-L, Shi C, Yu H-Q, Sheng G-P (2016) A novel TEMPO-mediated oxidized cellulose nanofibrils modified with PEI: preparation, characterization, and application for Cu(II) removal. *J Hazard Mater* 316:11–18. <https://doi.org/10.1016/j.jhazmat.2016.05.018>
- Zheng QF, Cai ZY, Gong SQ (2014) Green synthesis of polyvinyl alcohol (PVA)-cellulose nanofibril (CNF) hybrid aerogels and their use as superabsorbents. *J Mater Chem A* 2:3110–3118. <https://doi.org/10.1039/c3ta14642a>

**Publisher's Note** Springer Nature remains neutral with regard to jurisdictional claims in published maps and institutional affiliations.